UNIVERSITY OF AMSTERDAM

UvA-DARE (Digital Academic Repository)

Extreme ultraviolet patterning of tin-oxo cages

Haitjema, J.; Zhang, Y.; Vockenhuber, M.; Kazazis, D.; Ekinci, Y.; Brouwer, A.M.

DOI
10.1117/1.JMM.16.3.033510

Publication date
2017

Document Version
Final published version

Published in
Journal of Micro/Nanolithography, MEMS and MOEMS

License
CC

Link to publication

Citation for published version (APA):
Haitjema, J., Zhang, Y., Vockenhuber, M., Kazazis, D., Ekinci, Y., & Brouwer, A. M. (2017). Extreme ultraviolet patterning of tin-oxo cages. *Journal of Micro/Nanolithography, MEMS and MOEMS*, *16*(3), Article 033510. https://doi.org/10.1117/1.JMM.16.3.033510

General rights
It is not permitted to download or to forward/distribute the text or part of it without the consent of the author(s) and/or copyright holder(s), other than for strictly personal, individual use, unless the work is under an open content license (like Creative Commons).

Disclaimer/Complaints regulations
If you believe that digital publication of certain material infringes any of your rights or (privacy) interests, please let the Library know, stating your reasons. In case of a legitimate complaint, the Library will make the material inaccessible and/or remove it from the website. Please Ask the Library: https://uba.uva.nl/en/contact, or a letter to: Library of the University of Amsterdam, Secretariat, P.O. Box 19185, 1000 GD Amsterdam, The Netherlands. You will be contacted as soon as possible.

UvA-DARE is a service provided by the library of the University of Amsterdam (https://dare.uva.nl)

Download date:10 Sep 2026

Extreme ultraviolet patterning of tin-oxo cages

Jarich Haitjema,[a] Yu Zhang,[a] Michaela Vockenhuber,[b] Dimitrios Kazazis,[b] Yasin Ekinci,[b] and Albert M. Brouwer[a,c,*]
[a]Advanced Research Center for Nanolithography, Amsterdam, The Netherlands
[b]Paul Scherrer Institute, Villigen, Switzerland
[c]University of Amsterdam, Van't Hoff Institute for Molecular Sciences, Amsterdam, The Netherlands

Abstract. We report on the extreme ultraviolet (EUV) patterning performance of tin-oxo cages. These cage molecules were already known to function as a negative tone photoresist for EUV radiation, but in this work, we significantly optimized their performance. Our results show that sensitivity and resolution are only meaningful photoresist parameters if the process conditions are optimized. We focus on contrast curves of the materials using large area EUV exposures and patterning of the cages using EUV interference lithography. It is shown that baking steps, such as postexposure baking, can significantly affect both the sensitivity and contrast in the open-frame experiments as well as the patterning experiments. A layer thickness increase reduced the necessary dose to induce a solubility change but decreased the patterning quality. The patterning experiments were affected by minor changes in processing conditions such as an increased rinsing time. In addition, we show that the anions of the cage can influence the sensitivity and quality of the patterning, probably through their effect on physical properties of the materials. *© The Authors. Published by SPIE under a Creative Commons Attribution 3.0 Unported License. Distribution or reproduction of this work in whole or in part requires full attribution of the original publication, including its DOI.* [DOI: 10.1117/1.JMM.16.3.033510]

Keywords: tin-oxo cage; EUV lithography; EUV photoresist; interference lithography; organometallic photoresist.

Paper 17061P received May 4, 2017; accepted for publication Aug. 22, 2017; published online Sep. 15, 2017.

1 Introduction

Extreme ultraviolet lithography (EUVL) is a powerful technique, which can further improve the resolution of patterning in advanced semiconductor manufacturing. Nevertheless, there are still many challenges to be overcome for the introduction of EUVL into high volume manufacturing. One of these challenges is the photoresist performance. The high energy per photon means fewer photons for the same dose, which exacerbates stochastic noise.[1] This leads to increased line edge roughness and puts limits on the achievable resolution for a given dose. One way to get more chemical conversion per absorbed photon is to use chemical amplification mechanisms such as in acid-sensitive resists.[2] However, the photoacid generators and their quenchers are randomly distributed, causing further stochastic effects.[3] Quenchers, in particular, are known to have a large contribution to stochastic noise, as a result of their low concentration in the photosensitive layer.[4]

For these reasons, it is interesting to search for alternative materials with improved properties, such as metal-containing compounds. These have a larger absorption cross section for EUV photons than organic materials, which contributes to an increase in sensitivity.[5] This may eliminate the need for chemical amplification, removing statistical uncertainties in the position of photoacid generators and quenchers. Metal-containing compounds also have an improved etch resistance compared to conventional chemically amplified resists (CARs).[6,7]

Nanoparticles, introduced by Trikeriotis et al.,[7] and organic–inorganic hybrid compounds have demonstrated photoresist performance.[8,9] Since the latter materials are molecular, they are well defined with a single particle size, as opposed to the nanoparticle systems. Tin-oxo cages are the subject of the present work (see Fig. 1).[10] The cage has a 2+ charge and is therefore stabilized by one or two counterions.

The tin-oxo cage molecules can be regarded as the tin analog of the silicon-containing silsesquioxane class of compounds. Hydrogen silsesquioxane (HSQ) is the most prominent member of this family, and it has been used to achieve high-resolution patterning with both e-beam and EUV lithography.[11] However, the sensitivity of HSQ is very low, mainly due to the low EUV absorption. EUV absorption can be increased significantly by incorporating metal atoms that strongly absorb EUV light. It is not possible to directly replace silicon with tin in HSQ due to the larger size of the tin atom. However, the tin-oxo cage material is a similar building block with a slightly different shape. The calculated linear absorption coefficient (α) for TinS is 13.3 μm^{-1} assuming a density of 1.9 g/cm^3 taken from the crystal structure,[12] and using atomic EUV absorption coefficients reported in the literature.[13] In 2017, the absorption coefficients α for some of the tin cage materials were measured[14] and found to be in good agreement with the predicted ones.

The absorption coefficient α of organic polymer-based resists is typically $\sim 5\ \mu m^{-1}$, whereas tin-based materials from Inpria Corp. show higher absorption coefficients, even up to 20 μm^{-1}.[15] While a large absorption coefficient favors sensitivity, it is not known how efficiently absorbed photons induce a change in solubility of these materials, nor is it known what the maximum achievable efficiency is.

The tin-oxo cage system has the advantage that two properties can be readily altered: the anions at the side of the cage (X^-) and the organic groups (*n*-butyl chains in this case). In this study, we focus on the EUV patterning of some selected

*Address all correspondence to: Albert M. Brouwer, E-mail: F.Brouwer@arcnl.nl

Downloaded From: https://www.spiedigitallibrary.org/journals/Journal-of-Micro/Nanolithography,-MEMS,-and-MOEMS on 2/14/2018 Terms of Use: https://www.spiedigitallibrary.org/terms-of-use

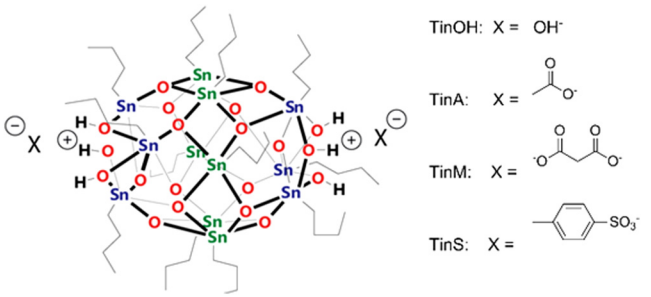

Fig. 1 Tin-oxo cages with four different anions: hydroxide (TinOH), acetate (TinA), malonate (TinM), and tosylate (TinS). For the malonate, the ratio of tin cages to malonate anions is 1:1.

materials of this class. The chemical changes upon exposure to short-wavelength UV light are discussed elsewhere.[16,17]

2 Materials and Methods

2.1 *Materials*

We synthesized the tin-oxo cage with two tosylates as the anions (TinS) according to a procedure described by Eychenne-Baron et al.[18] Butylstannoic acid hydrate ($BuSnOOH \bullet xH_2O$) was mixed with an excess of *p*-toluene sulfonic acid monohydrate ($pTsOH \bullet H_2O$) in a round bottom flask with toluene as a solvent. The reaction mixture was refluxed overnight under removal of water using a Dean–Stark apparatus. The resulting product was filtered using Celite to remove insoluble material. The toluene was then removed under reduced pressure to yield a white crude product, which was further purified by recrystallization from 1,4-dioxane. Needle-shaped white crystals were isolated.

The dihydroxide form of the tin cage (TinOH) was obtained using a procedure described by Eychenne-Baron et al.[18] A 20 wt. % solution of TinS in isopropanol (IPA) was mixed with a solution of aqueous tetramethylammonium hydroxide (TMAH) in IPA. The TMAH was used in excess (2.3×). Precipitation occurred instantaneously. The resulting suspension was filtered to obtain a white powder.

The diacetate (TinA) and malonate (TinM) forms of the tin cluster were obtained using a procedure described by van Lokeren et al.[19] The dihydroxide TinOH was dissolved in tetrahydrofuran (UvaSol, spectroscopic grade) after which two molar equivalents were added of glacial acetic acid (Aldrich), or one molar equivalent of malonic acid (purified by recrystallization), respectively. NMR analysis was carried out using a Bruker AV-400 NMR spectrometer. The ^{1}H and ^{119}Sn NMR spectra were found to be in agreement with the literature.[10,12,18] The thermogravimetric analysis (TGA) of TinOH was performed using a NETZSCH thermogravimetric analyzer, using 22.2 mg of sample in an Al_2O_3 crucible. Heating was performed from 35°C to 800°C at 10 K/min in an $80\%/20\%N_2/O_2$ atmosphere.

2.2 *Preparation of Thin Films*

For a typical thin film of ~40 nm thickness, a solution is made of 15 mg/mL of the tin-oxo cage (with any of the counterions) dissolved in toluene using sonication (30 s). The malonate form did not sufficiently dissolve in toluene and was therefore dissolved in methanol. Particulates were removed by filtering the solutions using a 0.2-μm syringe filter before spin coating. The solutions were spun on Si wafers (for interference lithography) and 2×2 cm^2 Si chips (for open-frame experiments) with a spin speed of 2500 rpm for 45 s, with a subsequent soft bake of 30 s at 90°C. Both wafers and chips were treated with hexamethyldisilazane (HMDS) before spin coating. After exposure, the samples were developed using a 2:1 IPA/H_2O mixture for 30 s and rinsed for 10 s.

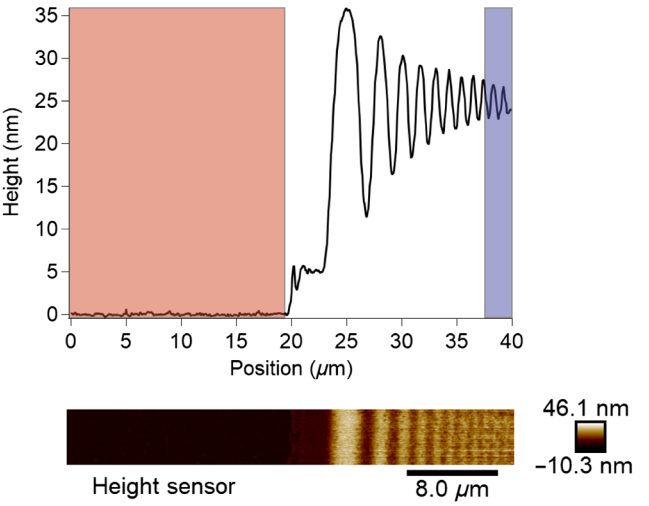

Fig. 2 AFM image of the material edge (bottom). Image height was corrected using a second-order flattening procedure. The height values of the image were then averaged along the *y*-axis to produce an edge cross section (top). The average substrate height (red) was compared with the average photoresist height far from the edge (blue).

2.3 *EUV Exposure*

EUV exposures were carried out at the XIL-II beamline of the Swiss Light Source (SLS) synchrotron at the Paul Scherrer Institute (PSI) with EUV light at $\lambda = 13.5$ nm.[20] For the open-frame experiments, 0.5×0.5 mm^2 areas were exposed to EUV light through a square aperture. For the patterning experiments, a transmission mask was used providing line/space patterns with pitches of 100, 80, 60, and 44 nm.

2.4 *Postexposure Analysis*

Atomic force microscopy (AFM) images were made using a Bruker Dimension Icon, using the PeakForce tapping (ScanAsysAir) mode. Perpendicular to the resist edge, fields of 40×5 μm^2 were scanned with 128 samples/line, using a scan speed of 0.5 Hz. The raw images were corrected for bowing using first- and second-order corrections, and the film thickness was measured by comparing the height of the film with the height of the substrate, as shown in Fig. 2. Scanning electron microscopy (SEM) imaging was performed using a Carl Zeiss SUPRA 55VP SEM with a voltage of 1 kV.

3 Results and Discussion

3.1 *Open-Frame Experiments: Contrast Curves*

Contrast curves (also known as H-D curves or characteristic curves) were obtained by measuring the remaining thickness

Downloaded From: https://www.spiedigitallibrary.org/journals/Journal-of-Micro/Nanolithography,-MEMS,-and-MOEMS on 2/14/2018 Terms of Use: https://www.spiedigitallibrary.org/terms-of-use

after development as a function of EUV exposure dose using AFM imaging (see experimental section).

A typical AFM image of the material edge is shown in Fig. 2. Here, the left part of the image is blank Si substrate, because the unexposed material was removed by the developer. The right part of the image shows exposed and therefore insoluble material. It can be seen that the edge of the profile is partly covered by a wave pattern, caused by interference effects (knife-edge effect). To measure the remaining thickness correctly, the height of the resist was measured as far from the edge as possible and averaged over a certain distance window.

Contrast curves were first used to compare compounds with different counterions, TinOH and TinA. The anion of the tin cage can not only alter the reaction of the material to EUV excitation[10] but also its physical properties such as solubility. For instance, doubly charged anions such as malonate combined with the cage compound render the material more polymeric in nature because the tin cage can form elongated chains with the doubly charged counterion.[19]

TinOH and TinA were spin coated with a subsequent postapplication bake (90°C) and exposure (see experimental). They did not differ significantly in their performance judging from the contrast curves (Fig. 3). This means that the anions are probably not directly involved in the mechanism that leads to the solubility switch. They could act as nonreactive spacers, as was proposed by Cardineau et al.[10] We can observe the onset of gelation at ~10 mJ/cm^2 and a maximum thickness at ~50 mJ/cm^2. At higher doses, the thickness decreases again. This is likely due to loss of more of the butyl chains, in analogy to the results of deep UV exposures.[16]

In addition to the anion effect, improvements to the process can also alter the contrast curves. In fact, photoresist parameters such as sensitivity and resolution are only meaningful concepts if the process conditions are optimized. Parameters that were optimized were: developer, development time, PAB, and PEB. First, the use of a different developer may improve resist performance because of a larger difference in the solubility rates of the exposed and unexposed areas. A few other developers instead of the 2:1 IPA/H_2O mixture[10] were tried, such as 2-heptanone.[21] None of them, however, seemed to significantly improve resist performance. We will therefore only show results obtained with the 2:1 IPA/H_2O developer.

Another important processing step is postexposure baking (PEB). This is well known for CARs: heating the resist after exposure allows diffusion of the photoacids and induces the removal of the dissolution inhibiting protecting groups.[22] For non-CARs, this connection is less clear. Although photoacid diffusion does not apply here, the heating could still induce additional chemical reactions of species that were formed during the exposure step. This is especially the case since EUV exposures take place in vacuum. The photoresist material is baked under ambient atmosphere, enabling reactions of reactive species with oxygen and moisture.

However, the conditions of the PEB should be carefully tuned, since the unexposed material may also change solubility. This can lead to loss of contrast. In the case of a negative tone resist, it is essential that the unexposed part can still be fully cleared by the developer.

The baking effect was studied for two different anions: the hydroxide and the malonate. The malonate form is more polymeric in nature and may, therefore, have a different response to heating. The effect of baking at 100°C for the hydroxide form is shown in Fig. 4.

PEB (100°C, 2 min) has a significant effect on the sensitivity of the tin-oxo cage material. A lower dose is required to reach the onset of gelation (7 mJ/cm^2 PEB, 8 mJ/cm^2 non-PEB) and to achieve a remaining thickness of 20 nm, the dose needed is 2× smaller. Additionally, the contrast seems to increase as the initial increase of remaining thickness with dose is ~4× larger for the baked samples. However, we note that the contrast measured in this way can be different from the theoretical contrast, which is defined as the difference in solubility rate between the exposed and nonexposed parts of the resist.[23] Measuring this more directly, for instance using a quartz crystal microbalance (QCM) would be needed to get an accurate value for the contrast.

The effect of baking was also investigated for a layer with higher initial thickness (60 nm instead of 40 nm). The baking effect was consistent here (see Fig. 5). However, we also note a large increase in the sensitivity for a thicker layer of TinOH. Only 2 mJ/cm^2 was needed for a reasonable

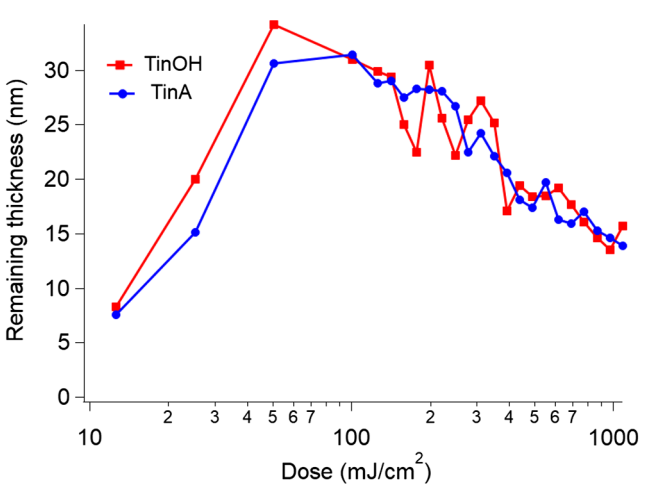

Fig. 3 Remaining layer thickness as a function of EUV dose for TinOH and TinA. Initial thickness was ~40 nm. No PEB was applied.

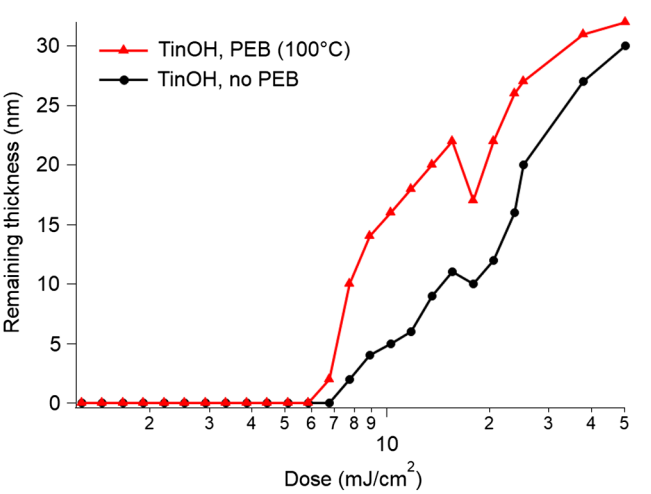

Fig. 4 Contrast curves of TinOH, measured without PEB (black) and with PEB at 100°C (red). Initial thickness was ~40 nm.

Downloaded From: https://www.spiedigitallibrary.org/journals/Journal-of-Micro/Nanolithography,-MEMS,-and-MOEMS on 2/14/2018 Terms of Use: https://www.spiedigitallibrary.org/terms-of-use

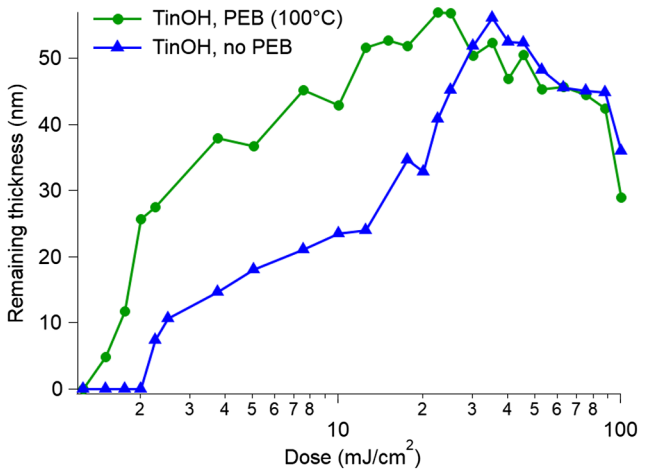

Fig. 5 The PEB effect for TinOH with a higher initial layer thickness (60 nm).

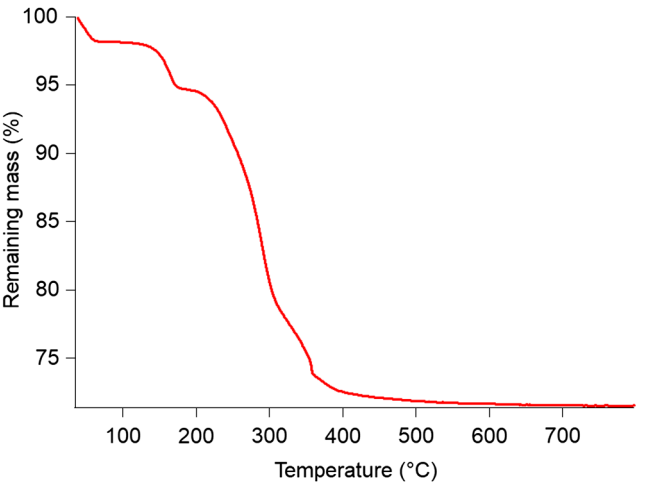

Fig. 6 TGA analysis for TinOH powder, in an 80%/20% N_2/O_2 atmosphere.

remaining thickness (26 nm). Calculations by others show that a reasonable dose at the bottom is required for this type of materials, in order to make the converted material attach to the substrate.[24] However, these results contradict this. Apparently, converted material attaches easily even if it is not in direct connection with the substrate. A thicker layer leads to a larger amount of converted material, which apparently leads to a higher remaining thickness as well. The effect of resist thickness was investigated earlier for CARs in previous work,[25] which also showed dependence of lithographic performance on layer thickness. For CARs, pattern collapse occurred more often upon increasing layer thickness (25 to 30 nm), though on the other hand, LER decreased. Pattern quality also worsened for tin cage material upon increasing layer thickness (results not shown).

The films were also postexposure baked at two higher temperatures: 120°C and 150°C. The unexposed parts of the film became partly insoluble. In the case of 120°C, the unexposed resist layer was still lower in height than the exposed material, except at very low doses (<5 mJ/cm^2). We suspect that, at these low doses, the shrinkage of the material was a larger factor than the solubility change. In the case of a 150°C PEB, the unexposed layer was barely soluble, leading to a decrease in height of the exposed parts for all used doses (2 to 50 mJ/cm^2). PEB at these higher temperatures is probably not suitable for patterning.

The effect of temperature on the materials was investigated by means of TGA, with which mass loss as a function of temperature can be measured. This can give additional information about the temperature stability of the unexposed material. A TGA curve of TinOH is shown in Fig. 6.

It can be seen that the remaining mass of TinOH first has a slight drop at the onset of the curve (<100°C). This can be attributed to the loss of some loosely attached IPA, the solvent that was used in the conversion step from TinS to TinOH (see experimental section). The remaining mass reaches a first plateau around 100°C, but drops suddenly above 150°C, at which temperature we observe a change in solubility. Banse et al.[26] reported that the crystal structure of TinOH contains four molecules of IPA, but they observed that powders are easily obtained that contain less IPA. The weight loss at ~150°C could be due to the loss of the most tightly bound solvent. It is also conceivable that water is eliminated, accompanied by deprotonation of the bridging OH-groups. Above ~200°C, a gradual loss of ~22% of the original weight occurs that can be attributed to the loss of organic content (cleavage of the butyl groups). The final remaining mass is 72%, which is close to the theoretical remaining mass of 73% assuming complete conversion to SnO_2. The slightly lower remaining mass can be attributed to the presence of IPA or H_2O in the initial sample.

Temperature response can be different for different tin cage materials. The malonate form (TinM) was also baked at 120°C. Surprisingly, the nonexposed TinM was still completely soluble even at this temperature. In addition, the sensitivity of the material seems to be high (see Fig. 7), although the high initial layer thickness also plays a role. If we compare the results to TinOH (Fig. 5), we see that in both cases a higher initial thickness leads to a higher remaining thickness. However, the measured contrast of TinM under these conditions appears to be lower than that of TinOH (PEB at 100°C, Fig. 5), which could explain why the patterning results of TinM were not significantly better.

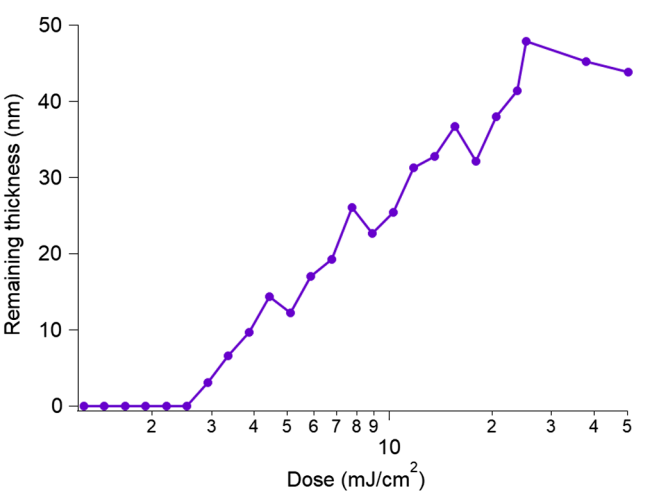

Fig. 7 Contrast curve of TinM, using a PEB of 120°C. Initial thickness was ~50 nm.

Downloaded From: https://www.spiedigitallibrary.org/journals/Journal-of-Micro/Nanolithography,-MEMS,-and-MOEMS on 2/14/2018 Terms of Use: https://www.spiedigitallibrary.org/terms-of-use

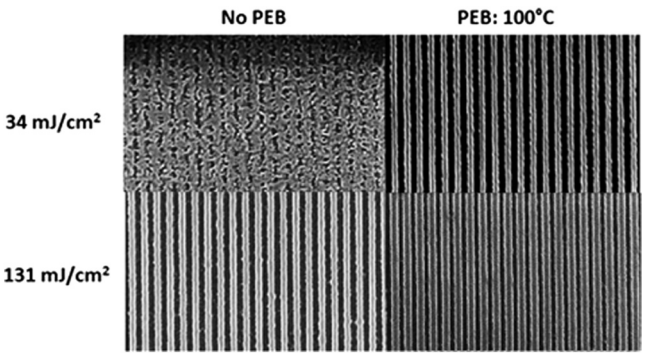

Fig. 8 The effect of PEB on TinOH measured at two different doses (34 and 131 mJ/cm^2) for 50-nm half-pitch lines.

3.2 *Interference Lithography Experiments: Patterning*

Line patterns were printed in ~30-nm-thick films of the tin cage materials using EUV interference lithography. Transmission diffraction gratings on a Si_3N_4 membrane were used (mask) to create mutually coherent beams, which in turn interfere to form the desired interference pattern. In our case, by utilizing two gratings we obtained line/space patterns with half the periodicity of the gratings on the mask.[27] Patterning experiments are important to demonstrate the potential of materials for photoresist applications: a performance is sought with the resolution and sensitivity being as high as possible, and the line edge roughness being minimized.

In Fig. 8, the effect of PEB can be seen. The pattern is almost invisible for the 34 mJ/cm^2 pattern, but clearly present when a postexposure bake (100°C, 30 s) is applied before development. In the case of the 131 mJ/cm^2 patterns, the lines increase in width with respect to the spaces. The lines are around 50 nm for the non-PEB sample but increase in width to around 68 nm for the PEB sample. This must mean that kinetically stable reaction products are formed during the EUV exposure, which reacts further during the PEB step.

Other parameters that were investigated were rinsing time and hard baking (postdevelopment baking). These parameters were investigated because they could have a favorable effect on microbridging, an undesirable phenomenon that was encountered during interference lithography experiments. The effect of rinsing and hard bake on this phenomenon is shown in Fig. 9.

The images show that the bridging effect is reduced if a longer rinsing time is used. Longer rinsing time also leads to smaller lines relative to the spaces. Under standard conditions, the lines are around 60 nm, whereas longer rinsing decreases this to around 50 nm. This implies that the resist is still partially soluble in the rinser (H_2O) and that the rinsing should not be performed for too long of a time. Hard baking (200°C for 1 min) does not significantly change the pattern, although it slightly reduces the line width to around 55 nm.

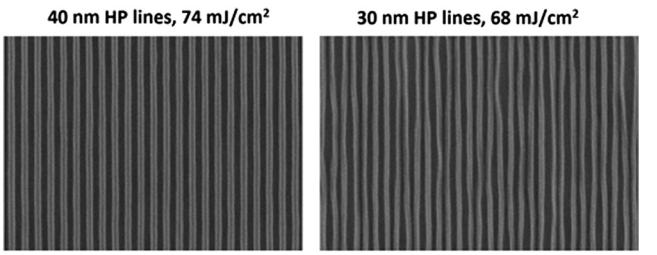

Fig. 10 Interference lithography on TinA. Processing conditions: PAB 90°C (1 min), PEB 100°C (1 min), and hard-bake 200°C (1 min).

The materials were also tested at a higher resolution. Although 80-nm pitch lines could be printed, the 60- and 44-nm pitch lines were significantly more difficult to print. Significant bridging between lines was observed. Probably this has to do with a problem of the development or rinsing process. Pattern collapse does not seem very likely, however, since the aspect ratio of the pattern is close to 1 : 1. Rather, the lines seem to detach from the substrate, signaling poor adhesion of the resist film or pattern collapse. For none of the presently studied materials, patterns at 22-nm HP could be resolved. Further investigations and improvements are needed to reach high resolution, such as reducing the aspect ratio, changing and optimization of the rinsing solvent, and improving adhesion of the resist to the substrate using surface treatments or underlayers.

Similarly to the open-frame experiments, we also patterned thicker layers (30 nm instead of 20 nm). However, a higher sensitivity was not found here. A reason could be that adhesion of the lines is very important for patterning experiments. A thicker layer receives less light at the bottom, making this adhesion more difficult.

The best patterns were created for the tin cage with acetate (CH_3COO^-) anions. This material was significantly less prone to pattern collapse or bridging, perhaps owing to its better stability. Two patterns at half pitches of 40 and 30 nm for this anion can be seen in Fig. 10. As it is seen in the figure, patterning with high quality is obtained down to 30-nm HP and the resolution is limited by the pattern collapse due to the adhesion problems.

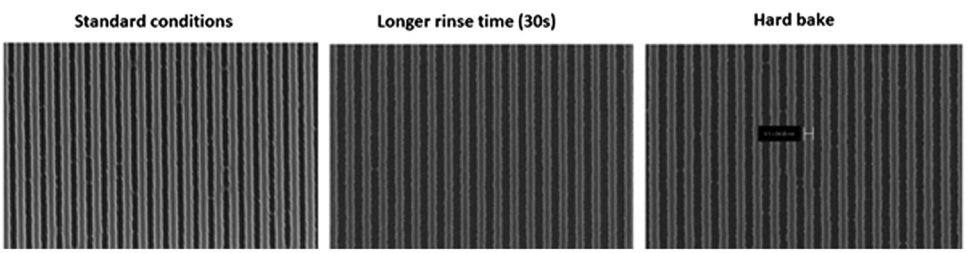

Fig. 9 Minimization of bridging effect, for TinOH using a dose of 110 mJ/cm^2 on 50-nm HP lines. The regular rinsing time was 10 s. PEB was performed at 100°C for 2 min for all three patterns. Hardbaking (postdevelopment baking) was performed at 200°C for 1 min.

Downloaded From: https://www.spiedigitallibrary.org/journals/Journal-of-Micro/Nanolithography,-MEMS,-and-MOEMS on 2/14/2018 Terms of Use: https://www.spiedigitallibrary.org/terms-of-use

4 Conclusion

We studied the EUV patterning of thin films of a small set of tin-oxo cage compounds. The relatively high packing density of Sn atoms provides a highly absorbing material,[14] since Sn is one of the elements most strongly absorbing at 13.5 nm.[13] Optimization of the processing conditions provided a better sensitivity than was reported previously.[10] Large area exposure (contrast curve) experiments showed a dependence on initial layer thickness and PEB temperature. Postexposure baking also substantially improved the negative tone photoresist performance in patterning experiments. This suggests that EUV photoreaction products are formed that can further react during the baking step. Identification of such photoproducts is a target of our ongoing research. Loss of carbon, in any form, leaves the Sn atoms in a coordinatively unsaturated state, making them potentially more reactive. While we have achieved progress, it is clear that further improvements are needed to make the materials competitive with the state-of-the-art EUV resists. The process of improvement would benefit greatly from a better understanding of the photochemical processes at work. For instance, the relatively low sensitivity suggests that loss mechanisms may be at play in which EUV photons are not converted into the desired solubility change. Reduction of these loss mechanisms could pave the way toward more sensitive resist materials.

Acknowledgments

Part of this work has been carried out at the Advanced Research Center for Nanolithography (ARCNL), a public-private partnership of the University of Amsterdam (UvA), the VU University Amsterdam (VU), the Netherlands Organisation for Scientific Research (NWO), and the semiconductor equipment manufacturer ASML. We thank Lianjia Wu (ARCNL) for performing the TGA analysis. Part of this work was performed at the SLS; this includes preliminary AFM results obtained at the Scanning Probe Microscopy Laboratory of LMN, PSI. We thank Elizabeth Buitrago and Roberto Fallica for helping with the experiments, and ASML for providing the initial access to EUVL experiments at PSI. This project has received funding from the EU-H2020 research and innovation program under grant agreement No. 654360 having benefitted from the access provided by PSI in Villigen within the framework of the Nanoscience Foundries and Fine Analysis Europe Transnational Access Activity.

References

1. P. Naulleau et al., "EUV resists: pushing to the extreme," *J. Photopolym. Sci. Technol.* **27**, 725–730 (2014).
2. M. Shirai and I. Tsunooka, "Photoacid and photobase generators: chemistry and applications to polymeric materials," *Prog. Polym. Sci.* **21**, 1–45 (1996).
3. P. Naulleau et al., "Studying resist stochastics with the multivariate Poisson propagation model," *J. Photopolym. Sci. Technol.* **27**, 747–750 (2014).
4. P. Naulleau et al., "Stochastics and EUV patterning in the 1x-nm regime," *J. Photopolym. Sci. Technol.* **6**, 747–750 (2016).
5. D. De Simone et al., "Metal containing resist readiness for HVM EUV lithography," *J. Photopolym. Sci. Technol.* **29**, 501–507 (2016).
6. K. Kasahara et al., "Recent progress in nanoparticle photoresist development for EUV lithography," *Proc. SPIE* **9776**, 977604 (2016).
7. M. Trikeriotis et al., "A new inorganic EUV resist with high-etch resistance," *Proc. SPIE* **8322**, 83220U (2012).
8. J. M. Amador et al., "Patterning chemistry of HafSOx resist," *Proc. SPIE* **9051**, 90511A (2014).
9. H. Nakagawa, N. Takehiko, and T. Nagai, "Recent EUV resists toward high volume manufacturing," *J. Photopolym. Sci. Technol.* **27**, 739–746 (2014).
10. B. Cardineau et al., "Photolithographic properties of tin-oxo clusters using extreme ultraviolet light (13.5 nm)," *Microelectron. Eng.* **127**, 44–50 (2014).
11. N. Mojarad, J. Gobrecht, and Y. Ekinci, "Beyond EUV lithography: a comparative study of efficient photoresists' performance," *Sci. Rep.* **5**, 9235 (2015).
12. C. Eychenne-Baron et al., "Reaction of butyltin hydroxide oxide with p-toluenesulfonic acid: synthesis, x-ray crystal analysis, and multinuclear NMR characterization of $\{(BuSn)_{12}O_{14}(OH)_6\}(4\text{-}CH_3C_6H_4SO_3)_2$," *Organometallics* **19**, 1940–1949 (2000).
13. B. L. Henke, E. M. Gullikson, and J. C. Davis, "X-ray interactions: photoabsorption, scattering, transmission, and reflection at E = 50–30,000 eV, Z = 1–92," *At. Data Nucl. Data Tables* **54**, 181–342 (1993).
14. R. Fallica et al., "Absorption coefficient and exposure kinetics of photoresists at EUV," *Proc. SPIE* **10143**, 101430A (2017).
15. R. Fallica et al., "Dynamic absorption coefficients of chemically amplified resists and nonchemically amplified resists at extreme ultraviolet wavelengths," *J. Micro/Nanolithogr. MEMS MOEMS* **15**, 033506 (2016).
16. Y. Zhang et al., "Photochemical conversion of a tin-oxo cage compound studied using hard x-ray photoelectron spectroscopy," *J. Micro/Nanolithogr. MEMS MOEMS* **16**, 023510 (2017).
17. J. Haitjema et al., "Photoreactions of tin oxo cages, model EUV photoresists," *J. Photopolym. Sci. Technol.* **30**, 99–102 (2017).
18. C. Eychenne-Baron, F. Ribot, and C. Sanchez, "New synthesis of the nanobuilding block $[(BuSn)_{12}O_{14}(OH)_6]^{2+}$ and exchange properties of $[(BuSn)_{12}O_{14}(OH)_6](O_3SC_6H_4CH_3)_2$," *J. Organomet. Chem.* **567**, 137–142 (1998).
19. L. van Lokeren et al., "Probing the anions mediated associative behavior of tin-12 oxo-macrocations by pulsed field gradient NMR spectroscopy," *J. Phys. Chem. C* **114**, 16087–16091 (2010).
20. N. Mojarad et al., "Single-digit-resolution nanopatterning with extreme ultraviolet light for the 2.5 nm technology node and beyond," *Nanoscale* **7**, 4031–4037 (2015).
21. S. Meyers et al., "Organometallic solution based high resolution patterning compositions and corresponding methods," U. S. Patent 2016/0116839 A1.
22. W. D. Hinsberg et al., "Chemical and physical aspects of the postexposure baking process used for positive-tone chemically amplified resists," *IBM J. Res. Dev.* **45**, 667–682 (2001).
23. C. A. Mack, "Lithographic optimization using photoresist contrast," *Microelectron. Man. Tech.* **14**, 36–42 (1991).
24. W. D. Hinsberg and S. Meyers, "A numeric model for the imaging mechanism of metal oxide EUV resists," *Proc. SPIE* **10146**, 1014604 (2017).
25. Y. Ekinci et al., "EUV resists towards 11 nm half-pitch," *Proc. SPIE* **9048**, 904804 (2014).
26. F. Banse et al., "Hydrolysis of monobutyltin trialkoxides: synthesis and characterizations of $\{(BuSn)_{12}O_{14}(OH)_6\}(OH)_2$," *Inorg. Chem.* **34**, 6371–6379 (1995).
27. N. Mojarad, J. Gobrecht, and Y. Ekinci, "Interference lithography at EUV and soft X-ray wavelengths: principles, methods, and applications," *Microelectron. Eng.* **143**, 55–63 (2015).

Jarich Haitjema studied chemistry at the University of Utrecht. He has done his master's thesis on donor-to-donor energy transfer in lanthanide systems in the group of A. Meijerink. In 2015, he joined Fred Brouwer's Group at ARCNL as a PhD student to work on photoresist chemistry in hybrid organometallic systems.

Yu Zhang is a PhD student in the Nanophotochemistry Group at ARCNL. Her project is mainly about developing new photoresist for EUVL and looking for the mechanism of the photochemical reactions of photoresists. She got her bachelor's degree in chemistry at Shandong University, China, in 2012. She got her master's in "Lab on Chip" research at Gachon University (South Korea) in 2014.

Michaela Vockenhuber received her diploma from the Higher Technical School Wien 10 in 1997. Since 2009, she worked at the Paul Scherrer Institute, Switzerland and Swiss Light Source in the field of EUV lithography. Prior, she has been working at TRIUMF Vancouver, Canada and at IMS Nanofabrication GmbH Vienna, Austria, where she has been involved in prototyping of ion projection lithography tools.

Dimitrios Kazazis received his PhD in 2009 from Brown University, USA, working on GeOI tunneling FETs. He did his postdoc until 2014 at CNRS-LPN near Paris, on suspended 2DEGs in III-V and QHE

Downloaded From: https://www.spiedigitallibrary.org/journals/Journal-of-Micro/Nanolithography,-MEMS,-and-MOEMS on 2/14/2018 Terms of Use: https://www.spiedigitallibrary.org/terms-of-use

metrology on graphene. Later he joined the Paris Observatory nanofabricating THz detectors. Since 2016, he works at the Paul Scherrer Institute, Switzerland, on advanced lithography and nanofabrication techniques. He has taught several courses at Brown and at Paris 7 University (Diderot).

Yasin Ekinci received his PhD from the Max Planck Institute for Dynamics and Self Organization in Göttingen, Germany, in 2003. Since 2009, he is a senior scientist at Paul Scherrer Institute. He is the head of the Advanced Lithography and Metrology Group in Laboratory for Micro- and Nanotechnology and manager of the XIL-II beamline at Swiss Light Source. He works on EUV interference lithography and lensless imaging along with other topics in nanoscience.

Albert M. Brouwer obtained his PhD in organic photochemistry at Leiden University in 1987, after which he joined the University of Amsterdam. In 2006, he was appointed professor. Research topics are molecular machines, solar fuels, and fluorescent probes. In 2014, he joined the Advanced Research Center for Nanolithography where he leads the Nanophotochemistry Group, working on the mechanisms of EUV-induced chemical reactions in photoresists.

Downloaded From: https://www.spiedigitallibrary.org/journals/Journal-of-Micro/Nanolithography,-MEMS,-and-MOEMS on 2/14/2018 Terms of Use: https://www.spiedigitallibrary.org/terms-of-use